*4th MASHCON, Hamburg - Uliczka et al. (eds) - © 2016 Bundesanstalt für Wasserbau ISBN 978-3-939230-38-0 (Online)*
*DOI: 10.18451/978-3-939230-38-0_23*

# SHALLOW WATER AND INTERACTION EFFECTS IN ECDIS REAL-TIME MOTION PREDICTION SYSTEM

**A Ozersky** and **E Rogozhina,** Transas Technologies, Russia

## SUMMARY

Modern ECDIS systems are often equipped with optional motion prediction system. Often such prediction systems do not calculate influence of shore and bottom profile, ship-ship and ship bank interaction and some other effects. Problems that must be solved during the implementation of a motion prediction system for shallow water manoeuvring go beyond engineering aspects of such system. Depths and other chart-acquired data should be automatically analysed to form the optimal environment for further calculations. Algorithms for motion prediction must be much faster than real-time simulation algorithms, considering that each relatively long predicted trajectory must be fully re-calculated every few seconds. To achieve the required performance, simplified mathematical models are suggested, analysed and partially validated using experimental data. Results from a bridge simulator installation of the prediction system demonstrated its potential use in education and manoeuvring in restricted and shallow waterways.

## NOMENCLATURE

| | | |
|---|---|---|
| $Q$ | Generalised velocity vector $[u \quad v \quad w \mid p \quad q \quad r]^T$ | |
| $P$ | Resultant forces vector $[X \quad Y \quad Z \mid K \quad M \quad N]^T$ | |
| $\eta$ | Generalised coordinate vector $[x \; y \; z \; \phi \quad \theta \quad \psi]^T$ | |
| $U$ | Body-fixed linear velocity $[u \quad v \quad w]^T$ | (m/s) |
| $W$ | Body-fixed angular velocity $[p \quad q \quad r]^T$ | (rad/s) |
| $F$ | Force in body-fixed coordinates $[X \quad Y \quad Z]^T$ | (N) |
| $L$ | Moment about body-fixed centre $[K \quad M \quad N]^T$ | (N m) |
| $\mu$ | Position vector of a point $[x \quad y \quad z]^T$ | (m) |
| $\Theta$ | Inclination Euler angles $[\phi \quad \theta \quad \psi]^T$ | (rad) |
| $\mu_c$ | Vector of ship centre of gravity | (m) |
| $D$ | Generalised inertia matrix 6×6 | |
| $D_R$ | Rigid-body inertia matrix 6×6 | |
| $D_A$ | Fluid Added Mass and Inertia matrix 6×6 | |
| $J_1$ | Euler angle rotation matrix 3×3 | |
| $J_2$ | Euler attitude transformation matrix 3×3 | |
| $I_0$ | Inertia tensor 3×3 | (kg m$^2$) |
| $I$ | Identity matrix 3×3 | |
| $S_s$ | Skew-symmetric matrix 3×3 | |
| $\Omega$ | Square matrix of generalised velocities 6×6 | |
| $m$ | Mass of ship | (kg) |
| $\rho$ | Density of water | (kg/m$^3$) |
| $g$ | Gravity acceleration | (m/s$^2$) |
| $\nabla$ | Volumetric ship displacement | (m$^3$) |
| $L_{pp}$ | Ship length between perpendiculars | (m) |
| $B$ | Ship breadth | (m) |
| $T$ | Ship draught | (m) |
| $C_B$ | Block coefficient | |
| $h$ | Water depth | (m) |
| $Fn$ | Length Froude number | |
| $Fh$ | Depth Froude number | |
| $H_w$ | Pressure measured in meters of water of water gauge | (m) |
| $S$ | Area of pressure field zone | (m$^2$) |
| $\alpha$ | Bottom incline angle | (rad) |
| $C_{BL}$ | Channel blockage factor | |
| $l_{tr}$ | Transversal distance to boundary | (m) |
| $C_{CFD}$ | Cross flow drag coefficient | |
| $n_p$ | Propeller revolutions | (s$^{-1}$) |
| $\gamma_R$ | Apparent wind angle | (rad) |
| $C_{XH}$ $C_{YH}$ $C_{NH}$ | Hull hydrodynamic coefficients | |
| $C_{XA}$ $C_{YA}$ $C_{NA}$ | Hull aerodynamic coefficients | |
| ECDIS | Electronic Chart Display and Information System | |
| VTS | Vessel Traffic Systems | |
| DOF | Degree of Freedom | |
| AIS | Automatic Identification System | |
| HDI | Hydrodynamic Interaction | |
| UKC | Under Keel Clearance | |

## 1 INTRODUCTION

Factors such as the increase in marine transport traffic and the growth of ships' dimensions create difficulties in ship handling and increase the probability of unexpected challenging situations which can affect safe navigation in congested waterways. The human factor is one of the most important which affects navigation safety. Reliable prediction of ship manoeuvrability may need water restrictions and other ship interactions under complicated environmental conditions to be taken into account, such as wind, waves or strong current. This may avoid collisions with obstacles or with the banks of narrow waterways.

Modern navigation systems are often equipped with a ship motion prediction system. These systems calculate

the future ship trajectory, considering the ship's motion model and some assumptions about steering commands. Assumptions on the steering commands can be rather simple (e.g. rudder and telegraph will be always in the same position as they are now), or very complex as defined by the ship's pre-defined route or manoeuvring plan.

The outcome of the prediction depends on the quality of the ship motion model, the number of effects covered by the model and the quality of the input data including environmental information.

Prediction systems can be used as a part of an ECDIS system, as a part of an onboard route/manoeuver planning tool, or as a part of an educational or simulation system. There are many examples of such systems including, for instance, prediction of manoeuvring indices in Nomoto's equation and sailed rudder angle from AIS data [1], prediction systems with complex manoeuver planning tools, actual manoeuvring limits and area estimation [2, 3], fuzzy algorithm of collision avoidance in shallow confined waterway [4]. In 2010-2011, the prediction system based on the ship mathematical model was also implemented in Transas Navi-Sailor for the Stena Germanica III passenger ship. The system employed a 6DOF ship model used for navigational training and considered ship controls state, weather and water depth. It was found that ignoring interaction effects may confuse operators and potentially lead to wrong decisions.

In this paper, a prediction system that in addition to usual deep-water simulation considers shallow and restricted water effects, hydrodynamic and mechanical interaction with nearby objects and propeller wash interaction will be described. An overview of the human-machine interface between the system and its users and will be also provided.

## 2 DATA SOURCES FOR SHIP MOTION PREDICTION

The primary data for the prediction system are orders and the actual state of the ship's rudders, engines and thrusters.

Ship-bank and ship-ship hydrodynamic interaction effects require additional information sources to estimate influence on ship trajectory. For ship-bank interaction forces, such information sources are usually high quality S-57 charts or other official charts available for an area. Charts of required quality are sometimes not included in chart folios and can be received from local port authorities. Available 2D chart data is converted into the 3D environment and then analysed to predict ship-bank interaction forces.

For ship-ship interaction forces, it is necessary to obtain information about another ship manoeuvres and plans. If two ships and shore stations can be connected using e-Navigation digital channels, then the information exchange can be more complete, as shown in figure 1. The information can include a motion model of another ship or even the complete online trajectory prediction calculated by the target ship's ECDIS or VTS system.

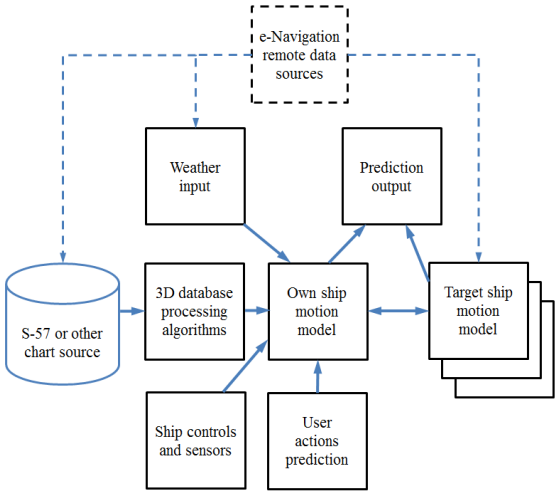


**Figure 1. Information exchange in prediction system. Dashed lines represent future potential for e-Navigation systems.**

Other information vital for online trajectory prediction is weather conditions. While weather information at the ship position can be acquired using the ship's own sensors, the information along the future trajectory is usually not known and should be estimated. The estimation can be made either as constant (e.g. constant wind value along the future trajectory) or using some simplified predictions (e.g. simplified wind shadowing algorithms if 3D models of surrounding area and ships are available). Sometimes this information can be pre-calculated using shore computers, as shown in [5]. In the future, when e-Navigation tools and cheap arrays of sensors will become widely available, such information could also be delivered online from shore VTS systems.

## 3 PREDICTOR MATHEMATICAL MODEL DESCRIPTION

### 3.1 COORDINATE FRAMES AND NOTATIONS

The following Cartesian coordinate frames are used to determine the position and orientation of a ship in 6 DOF, as shown in figure 2:

- Earth-fixed inertial reference frame $X_0Y_0Z_0$ with $O_0$ origin in a certain fixed point
- Body-fixed moving frame XYZ with C origin in the ship centre of gravity
- Local frame $X_lY_lZ_l$ fixed to the equilibrium state with C origin. Axis obtained by translating $X_0Y_0Z_0$ earth-fixed coordinate system parallel to itself until its origin coincides with the origin of the body-fixed coordinate system.

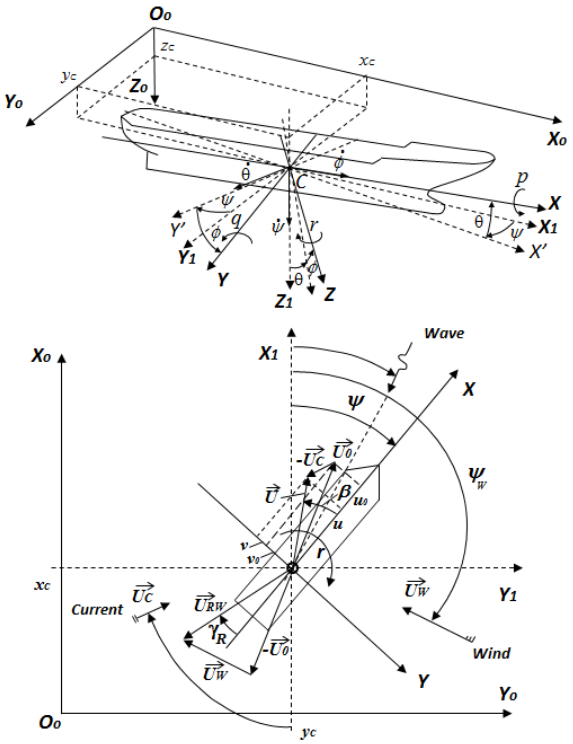


**Figure 2. Coordinate frames and sign conventions.**

The earth fixed coordinate system $X_0Y_0Z_0$ is used to describe the ship trajectory and orientation. The ship's motion and forces acting on the ship are described in the body-fixed coordinate frame XYZ.

## 3.2 SHIP MOTION EQUATIONS

Kinematic equations of motion for linear and angular velocities in compact form are as follows [6].

$$\begin{aligned} \dot{\mu_C} &= J_1(\Theta)U \\ \dot{\Theta} &= J_2(\Theta)\mathrm{W} \end{aligned} \tag{1}$$

Here $\mu_C = [x_C, y_C, z_C]^T$ are the coordinates of the centre of gravity in body-fixed reference frame, $J_{1\,3\times3}$ and $J_{2\,3\times3}$ denote transformation matrixes between Local and body-fixed reference frames. $J_1$ is Euler angle rotation matrix, $J_2$ is Euler angle attitude transformation matrix.

The ship dynamic equations of motion based on Newton's 2nd law of motion written in a compact matrix-vector form in the body-fixed reference frame according to [7] are:

$$D\dot{Q} + \Omega D Q = P \tag{2}$$

Here $P$ denotes total vector of external forces, $D$ is the generalised inertia matrix defined as the sum of rigid-body inertia matrix $D_{R\,6\times6}$ and fluid Added Mass and Inertia matrix $D_{A\,6\times6}$, which determines the kinetic energy of the surrounded fluid. $\Omega$ is the square matrix of generalised velocities, which can be written as a combination of skew-symmetric matrixes $S_S$ for linear and rotational velocities.

$$D = D_R + D_A \tag{3}$$

$$D_R = \begin{bmatrix} m\,I & -m\,S_S(\mu_C) \\ m\,S_S(\mu_C) & I_0 \end{bmatrix} \tag{4}$$

$$\Omega = \begin{bmatrix} S_S(\mathrm{W}) & 0 \\ S_S(U) & S_S(\mathrm{W}) \end{bmatrix} \tag{5}$$

Where m is the ship mass, $I_{3\times3}$ is the identity matrix and $I_{0\,3\times3}$ is the inertia tensor. The matrix products of $\Omega D$ in equation (2) gives Coriolis and Centripetal terms. The matrix-vector equation (2) forms the six scalar equations and together with the kinematic equations (1) gives a complete equations system to be solved for ship 6DOF motion simulation. The system can also be supplemented by a propulsor-engine dynamics equation.

Solution of the equation (2) yields ship velocities $Q$ in body-fixed reference frame. The ship's trajectories and location $\eta$ are obtained by integrating the kinematic equations (1) over time.

In the predictor model the set of ship motion equations can be calculated for 300 seconds in advance with the maximum integrational time step equal to 1 second. The motion model can be easily adapted to lower DOF simulation by excluding the corresponding DOF from the equations.

## 3.3 EXTERNAL FORCES

The total external vector $P$ includes buoyancy force, restoring and damping moments, the mechanical interaction and hydrodynamic forces in calm water as well as various environmental exciting forces due to wind, currents, waves shallow water effect, interaction with other ships, etc.

### 3.3 (a) Hull hydrodynamic Forces

The general structure of hydrodynamic force components of the ship hull for arbitrary motion in horizontal plane is considered as the sum of two non-linear functions of drift angle and yaw rate. The hydrodynamic coefficients are non-dimensionalised using density of water $\rho$, the reference area $L_{pp}T$, the reference length $L_{pp}$, squared linear velocity $U^2$ and squared generalised velocity $U^2 + r^2 L_{pp}^2$.

$$\begin{bmatrix} X_H \\ Y_H \\ N_H \end{bmatrix} = \frac{\rho}{2} L_{pp} T \left( \begin{bmatrix} C_{XH}\left(v,u,Fn,\frac{h}{T}\right) \\ C_{YH}\left(v,u,\frac{h}{T}\right) \\ L_{pp}C_{NH}\left(v,u,\frac{h}{T}\right) \end{bmatrix} U^2 + \begin{bmatrix} C_{XH}\left(v,u,r,\frac{h}{T}\right) \\ C_{YH}\left(v,u,r,\frac{h}{T}\right) \\ L_{pp}C_{NH}\left(v,u,r,\frac{h}{T}\right) \end{bmatrix} \left(U^2 + r^2 L_{pp}^2\right) \right) \tag{6}$$

The first parts are referred to as longitudinal force $C_{XH}\left(u,v,Fn,\frac{h}{T}\right)$, lateral force $C_{YH}(u,v,\frac{h}{T})$ and yawing moment $C_{NH}(u,v,\frac{h}{T})$ coefficients caused by pure drift motion. The second parts $C_{XH}\left(v,u,r,\frac{h}{T}\right)$, $C_{YH}(u,v,r,\frac{h}{T})$ and $C_{NH}(u,v,r,\frac{h}{T})$ express the corresponding compo-

nents arising from both yaw rate and drift. The coefficients also depend on load conditions. The shallow water effect is taken into account by means of the multiplicative exponential functions of relative depth $^{h}/_{T}$. These functions are individually applied to the hydrodynamic derivatives as ratios of shallow to deep water values in order to scale the hydrodynamic coefficients [8, 9].

The hydrodynamic coefficients can be derived from approximations proposed by Krylov State Research Centre [8], MMG group [10] as well as from model basin measurements performed in rotating arm facilities and planar motion mechanisms or can be precomputed using CFD methods. The system identification technique on the basis of full-scale trials is also applied. Therefore, a particular ship model can be adjusted according to any trial data available for a given ship.

In the mathematical model the above-mentioned coefficients are represented as multi-dimensional surfaces of draft, trim angle, drift angle, generalised trajectory curvature and $^{h}/_{T}$ ratio. An example of the total lateral force coefficient in deep water is presented in figure 3.A.

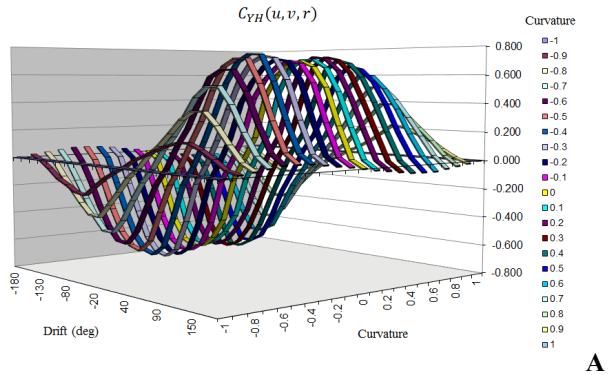


A

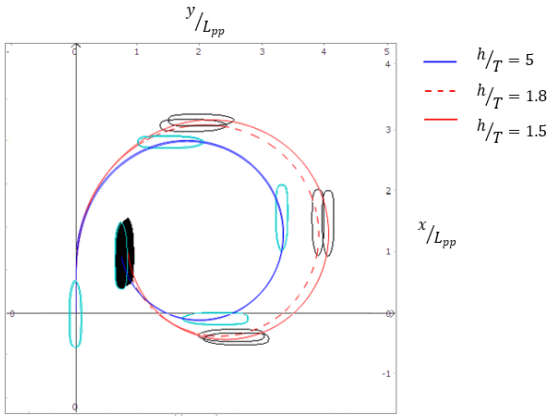


B

**Figure 3. A – Total sway force coefficient referred to squared generalised velocity. B – Comparison of the predicted trajectories of turning circle with rudder angle 35° at different h/T.**

The mathematical model of ship motion at shallow water also accounts for increasing inertial added masses and damping forces with decreasing water depth.

An example of simulation results of turning circle maneuvers both in deep and shallow water for the model described below in Table 1 is presented in figure 3.B with relative depths $^{h}/_{T}$ equal to 5, 1.8 and 1.5.

### 3.3 (b) Rudder and Propeller Forces

The rudder is considered as a low aspect ratio wing influenced by propeller induced flow and hull wake flow which gives flow-straightening effects. The forces and moments induced by the rudder are characterized by lift and drag coefficients, the rudder deflection angle and the actual slipstream and freestream areas with the corresponding effective velocities over the rudder. The rudder hydrodynamic coefficients are also functions of $^{h}/_{T}$ ratio.

The hydrodynamic forces induced by the propeller are computed using the common representation of propeller thrust and torque coefficients given in four quadrants versus a modified advanced coefficient, in order to cover all possible combinations of axial and rotational motions for arbitrary manoeuvres.

The influence of the shallow water on the propeller action is considered indirectly by changing the thrust deduction factor and wake fraction. The change of the lateral force on the rudder is considered to be dependent on the propeller operating conditions and, consequently, on the flow speed behind the propeller.

### 3.3 (c) Wind Forces

The wind model provides the continuous increase of the natural wind with the height above the sea level. The profile of the true wind is correlated with the Beaufort scale and determined by the average wind velocity given for the standard height of 10 metres. Wind forces and moments acting on the moving ship are computed from the apparent wind profile which is considered as a superposition of the uniform approaching $-\vec{U}_s$ and gradient $\vec{U}_a$ flows.

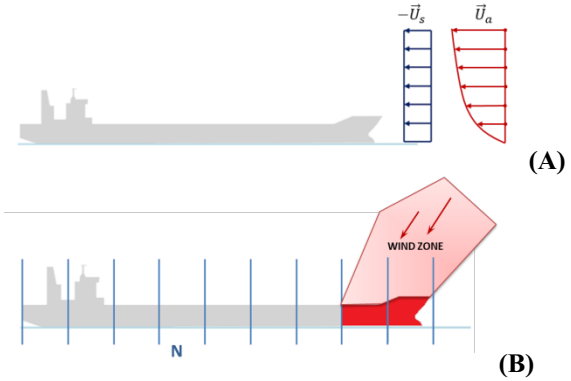


(A)

(B)

**Figure 4. A – profiles of wind gradient flow and relative flow. B – Container ship exposed to the wind local load at bow.**

Non dimensional wind force coefficients $C_{XA}$, $C_{YA}$, $C_{NA}$ given for the entire range of apparent wind angle $\gamma_R$ obtained from wind-tunnel tests or from known approximations are used according to [11].

The model also allows consideration of the apparent wind non-uniformity and gusts impact over the hull length. The underwater hull is divided into *N* sections as shown at figure 4.B; for each section the apparent wind profile is computed. The wind additional forces are predicted from the areas of the sections exposed to the local wind load.

3.3 (d) Current Forces

The current model is quite similar to wind force calculation. The current model allows the ship's motion to be modelled in complex hydrographic conditions: bends of river beds and channels, port approaches within the port areas with tidal currents, channel junction areas, etc.

The current is considered as a stationary flow with given velocity distribution in horizontal and vertical directions. The current vector interpolated by the local speed and direction is set at certain reference points on a chart, accounting for variables in depth current.

Forces and moments due to current computed in the body fixed reference frame are represented by two components. The first component as a part of the total current force on the hull depends on the mean current velocity $\overline{U}_c$ calculated over the ship hull.

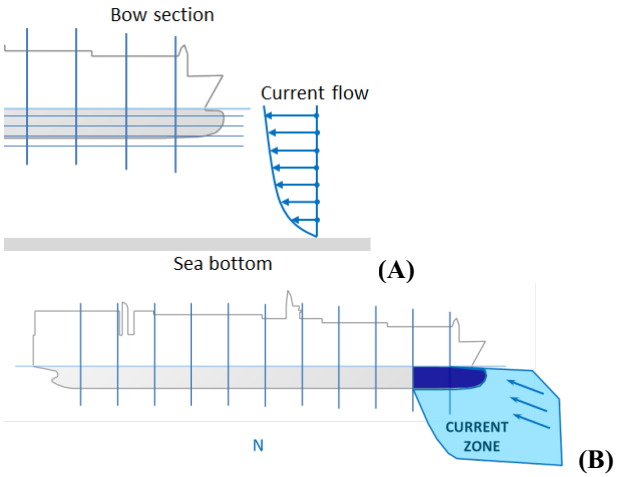


**Figure 5. A – profile of current gradient flow. B – Cruise ship exposed to the current local load at bow.**

The second component calculates the non-uniformity of the transversal local current speed $v_c(x)$ along the ship length. The additional sway force and yaw moment can be written as follows:

$$Y_c = -\frac{\rho}{2}\int_{-L/2}^{L/2} T(x)C_{CFD}(x)(v_c(x)-\overline{v_c}) \cdot |v_c(x)-\overline{v_c}|\,dx \quad (7)$$

$$N_c = -\frac{\rho}{2}\int_{-L/2}^{L/2} T(x)C_{CFD}(x)(v_c(x)-\overline{v_c}) \cdot |v_c(x)-\overline{v_c}|x\,dx \quad (8)$$

where $T(x)$ is variable draft along the hull, $C_{CFD}(x)$ is cross flow drag coefficient.

3.3 (e) Hydrodynamic Interaction Forces

Ship-to-ship and ship-to-bank effects modelling is based on taking into account the pressure field induced by other moving ships or pressure field modification in the vicinity of channel walls, moored ship, short pier, inclined bottom, under water shoals and jetties.

In order to provide accelerated-time computations the pressure distribution about the moving ship is approximated by simple geometrical zones. Positive pressure zones are located forward and aft, low pressure zone are located amidships. Each zone is represented in the ship motion model data by two semicircles of a given radius and a location centre. The aft zone also includes a sector of circle which reflects the low pressure wake field as well as the propeller action effect.

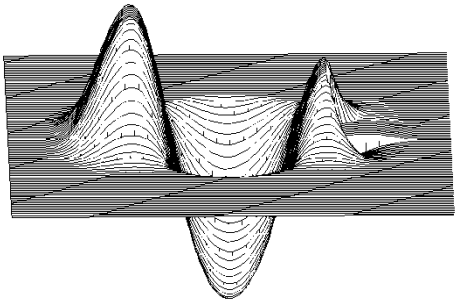

**Figure 6. The example of pressure field induced by a river-sea ship.**

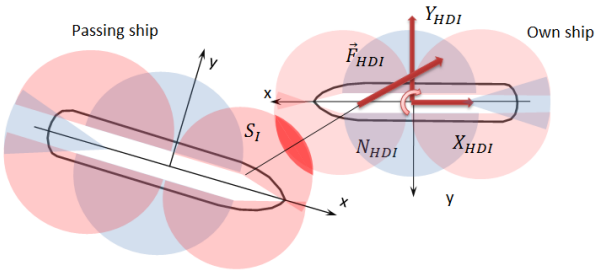


**Figure 7. HDI forces computational scheme.**

Excessive pressure induced by the moving ship is approximate in the motion model as pressure in metres of water gauge related to the corresponding geometrical zone.

The resultant pressure field $H_w$ in point with coordinated $\mu\,(x, y)$ considered as a sum of the following components.

$$H_w(\mu) = H_w(Fn, \mu) + H_w(v, r, \mu) + H_w{}^{wake}(u, v, r, n_p) \quad (9)$$

Here $n_p$ is propeller revolutions.

The first one corresponds to straight ahead or astern motion and depends on hull geometry and Froude number $Fn$. Maximum values of water gauge height $H_w$ corresponds to a zone origin and then steady decrease from the origin to the zone periphery. The second component reflects the influence of drift and yaw rate on the pressure field, taking into account relative transversal speed distribution in a lateral direction. The third component considers wakeflow and the main propeller induced jet.

An example of water gauge height $H_w$ distribution in body fixed reference frame for pressure field induced by a river-sea ship running straight ahead at constant speed in calm unrestricted water is shown on figure 6.

For computation of HDI forces, loop searches for geometrical intersection between each of the own ship zones $S_{own}$ and each of the other passing ships' zones $S_{passing}$ are performed. If intersection area $S_I^i$ is found the force $F_{HDI}$ is applied from the passing ship to own ship along the line linked by two origins of the corresponding intersected zones (figure 7).

$$F_{HDI} = S_{own} \bigcap_{i}^{N} S_{passing} \left[ \rho g \int_{S_I^i} \left( H_w(\mu_I^i) \right) ds \right] \quad (10)$$

Here $N$ denotes a number of the intersected zones and $\mu_I^i$ is a centre of the intersected area.

The total HDI longitudinal $X_{HDI}$ and transversal $Y_{HDI}$ forces are obtained by projecting $F_{HDI}$ to the corresponding axis. For yawing moment $N_{HDI}$ computation the point of force application is considered to be in the intersection of the line linked two origins and the ship centre plane.

To define the influence of waterways conjunctions on hydrodynamic forces, the vicinity of the ship is divided by longitudinal and transversal cross-sections to regular mesh with rectangular cells. Each cell with lateral and transversal indexes $i, j$ has area $S^{ij}$ and centre point $\mu_{ij}^G = \left[x_{ij}^G, y_{ij}^G, z_{ij}^G\right]^T$ In the centre point of each cell at every computational time step the water gauge height $H_w^{ij}$, water depth $h^{ij}$, shortest distances to boundaries, etc. are received from the map and translated to body-fixed frame XYZ.

The pressure field in each cell determined by the water gauge height $H_w^{ij}$ is corrected by influencing function $f_{BI}$ of the local Froude number with respect to water depth $Fh^{ij}$, local water depth ratio $h^{ij}/_T$, local sea bottom incline angle $\alpha_i$, local channel blockage factor $C_{BL}^i$ and local transversal distance to boundary $l_{tr}^{ij}$.

The influencing dependencies were empirically obtained and validated on the basis of an integrated theoretical and empirical approach using numerical analysis and the results of specially designed small scale self-propelled ship model tests [12, 13].

Hydrodynamic bank interaction forces are determined as the difference between forces in unrestricted and constrained conditions. Below are formulas for transversal force $Y_{BI}$ and yawing moment $N_{BI}$.

$$Y_{BI} = \rho g \left( \sum_i \sum_j sign\left(y_{ij}^G\right) \left( H_w^{ij} \cdot f_{BI}\left(Fn, Fh^{ij}, h^{ij}/_T, \alpha_i, C_{BL}^i\right) S^{ij} - H_w^{ij} S^{ij} \right) \right) \quad (11)$$

$$N_{BI} = \rho g \left( \sum_i \sum_j x_{ij}^G\, sign\left(y_{ij}^G\right) \left( H_w^{ij} \cdot f_{BI}\left(Fn, Fh^{ij}, h^{ij}/_T, \alpha_i, C_{BL}^i\right) S^{ij} - H_w^{ij} S^{ij} \right) \right) \quad (12)$$

The mathematical model also takes into account the influence of jets induced by other ships' propulsors. A jet from an external propeller or a thruster is modelled as a layer of local current.

It is important to note that this rough approach was developed as a compromise between accuracy and the computation speed appropriate for faster than real time computations. The model can be tuned to comply with basin experiments or with more advanced computational methods.

### 3.3 (f) Squat Forces

For accelerated time usage of the predictor, squat computations are based on the various simple empirical formulas used in practice, such as Romisch, Tothill, Barrass and the others [14]. During previous years Transas had performed analysis of the various empirical formulas used in marine practice and test measurements from the numerous sources and had developed sinkage and trim formulation for simulator real time use [15]. While such methods often over-predict squat, for better coincidence with real squat measurements or advanced time consuming computations the sinkage and trim formulation can be adopted for the particular ship model, by means of individual coefficients.

Squat parameters in the predictor are represented as precomputed data set. Considering that another squat formula, results of CFD experiments, model basin or full-scale measurements can be entered as a source for squat database for a ship model.

At each computational time step, bow sinkage and stern sinkage in metres are computed from current speed, depth and channel profile. Further on the base of precomputed data of buoyancy coefficient and restoring pitching moment versus relative submergence and pitch

the vertical force and pitching moment from the squat effect are computed and implemented into model.

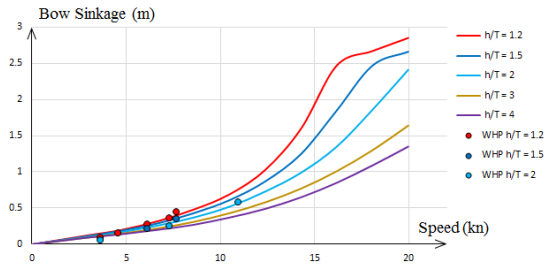


(A)

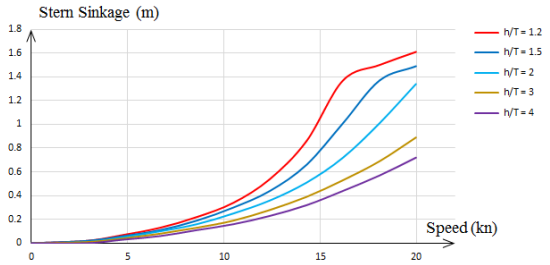


(B)

**Figure 8. Bow (A) and stern sinkage (B) in metres versus speed.**

In figure 8 the simulation results of squat bow and stern sinkages on shallow water are shown according to the Romisch prediction method for the model of container ship used in the bridge simulator exercise described below. Ship parameters are listed in table 1. These predicted results of the bow sinkage are compared with data from wheelhouse posters of similar containerships scaled according to the ship dimensions.

**Table 1. Main Particulars of Container ship**

| | |
|---|---|
| Displacement, ∇, $m^3$ | 32921.8 |
| $L_{pp}$, m | 190 |
| B, m | 30 |
| T (full load), m | 8.5 |
| Engine Diesel, MW | 17.3 |
| Propeller | FPP |
| Maximal speed, kts. | 20.1 |

### 3.4 ANALYSIS OF 3D BOTTOM SURFACE

Conversion of 2D electronic chart data into 3D bottom outline is performed automatically using triangulation, as shown on the figure 9. The depth and height marks, together with isobaths and some other map objects are treated as input. The output of triangulation is a set of 3D points connected with lines, together forming a mesh made of triangles.

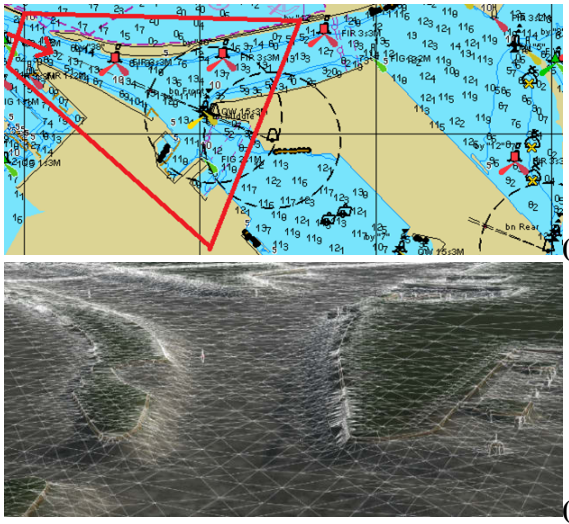

(A)

(B)

**Figure 9. Example of automatic conversion from S-57 chart (A) into 3D surface (B). The red trapezoid on the left shows the field of view of the 3D picture.**

This mesh comes through additional processing to identify parameters important for ship-bank interaction:

- average depth near ship
- distances to banks
- channel profile
- 3D surface shape to evaluate ship-bank interaction forces
- water flow restriction coefficient, which can also be interpreted as channel blockage factor.

The water way parameters required from the electronic chart are refreshed in the motion model's body-fixed reference frame every second or every time when ship position changes more than 0.1 of its length.

## 4 MODEL VALIDATION

The kinematic parameters and trajectories of ship-to-ship and ship-to-bank interaction were validated by specially designed model experiments [12, 13].

In order to distribute some particular results of model basin measurement onto the collection containing ships of varied types and dimensions, similarity criteria have been proposed [12] and an algorithm of the automated selection of model pairs has been developed. The satisfaction of the criteria enables the required geometric and dynamic similarity between small scale self-propelled test-tank models and full scale mathematical ship models in similarly investigated conditions.

### 4.1 SHIP-TO-SHIP HYDRODYNAMIC INTERACTION

Below is an example illustrating a comparison of behaviour of the ship mathematical models with the tank-test experimental results for similar models and navigational conditions for the overtaking manoeuvre on crossing courses.

In the simulated test the Container ship model also used in the predictor experiment below, sailing initially ahead by 0.6L, is overtaken by the Car Carrier ship.
The main particulars of the model used in the comparative tests are displayed in table 2.

**Table 2. Main Ship particulars and test conditions**

| | Transas | | Experiment | |
|---|---|---|---|---|
| Model | Container ship | Car carrier | TCH | CPT |
| $\nabla$, m$^3$ | 32921.8 | 68217.4 | 0.96 $10^{-3}$ | 1.73 $10^{-3}$ |
| $L_{pp}$, m | 181.5 | 228.9 | 0.477 | 0.592 |
| B, m | 30 | 36.2 | 0.094 | 0.12 |
| T, m | 8.5 | 10.88 | 0.0385 | 0.048 |
| Initial $x_c$, m | 155.07 | -20.74 | 0.4 | -0.05 |
| Initial $y_c$, m | 370.08 | 250.18 | 1.19 | 0.81 |
| Course, deg | -7.74 | -6.09 | -9.57 | -7.53 |
| Speed, m/s | 8.07 | 9.82 | 0.6 | 0.73 |
| $h/T$ | 5.87 | 4.59 | 5.97 | 4.79 |
| $Fn$ | 0.19 | 0.21 | 0.28 | 0.3 |
| $Fh$ | 0.36 | 0.44 | 0.4 | 0.48 |

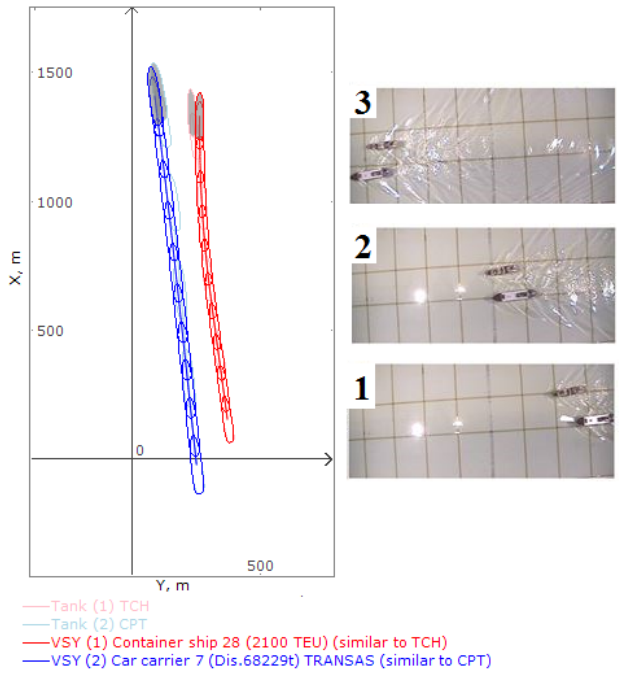


**Figure 10. Comparison of the simulated trajectories for overtaking manoeuvre against model basin measurements for similar models.**

The trajectories of the mathematical models shown in figure 10 obtained in this test are in qualitative agreement with the trajectories recorded in the tank test for the pair of models satisfying the similarity criteria.

## 4.2 HYDRODYNAMIC FORCES INDUCED BY PASSING SHIPS

The ship motion model was validated by a comparison with published results from passing ship model test for the open water case. It is known that the passing-ship-induced forces and moments can produce large motion responses of the moored ship, causing it to move along and away from the pier. These motions can damage cargo hoses, loading arms, gangways and ramps.

Figure 11 shows a comparison of the calculated external loads on the moored tanker induced by the passing tanker with the experiment [16]. The speed of the passing tanker is 7 knots; distances between the passing tanker and the moored tanker are 30, 60 and 120 metres, measured board to board. Path and course of the passing tanker were parallel to the moored tanker.

Loads on the moored tanker are related to the position of the passing tanker relative to the moored tanker.
The comparison with Remery's results are good enough: the shapes of the plots are almost identical, the values for peak and trough values for X, Y, and N predicted by the ship motion model are all essentially the same as those measured and predicted by Remery.

**Table 3. Ship particulars for interaction comparison.**

| | Transas | | Experiment (scale 1 : 60) | |
|---|---|---|---|---|
| | Moored Vessel | Passing Vessel | Moored Vessel | Passing Vessel |
| Ship type | Tanker | Tanker | Tanker | Tanker |
| $\nabla$, m$^3$ | 104000 | 131000 | 118800 | 129600 |
| $L_{pp}$, m | 239 | 270 | 257 | 250 |
| B, m | 44 | 49.9 | 36.8 | 40.4 |
| T, m | 12.2 | 12.2 | 15.7 | 15.2 |
| $h/T$ | 1.15 | 1.15 | 1.15 | 1.15 |
| $C_B$ | 0.81 | 0.8 | 0.8 | 0.85 |

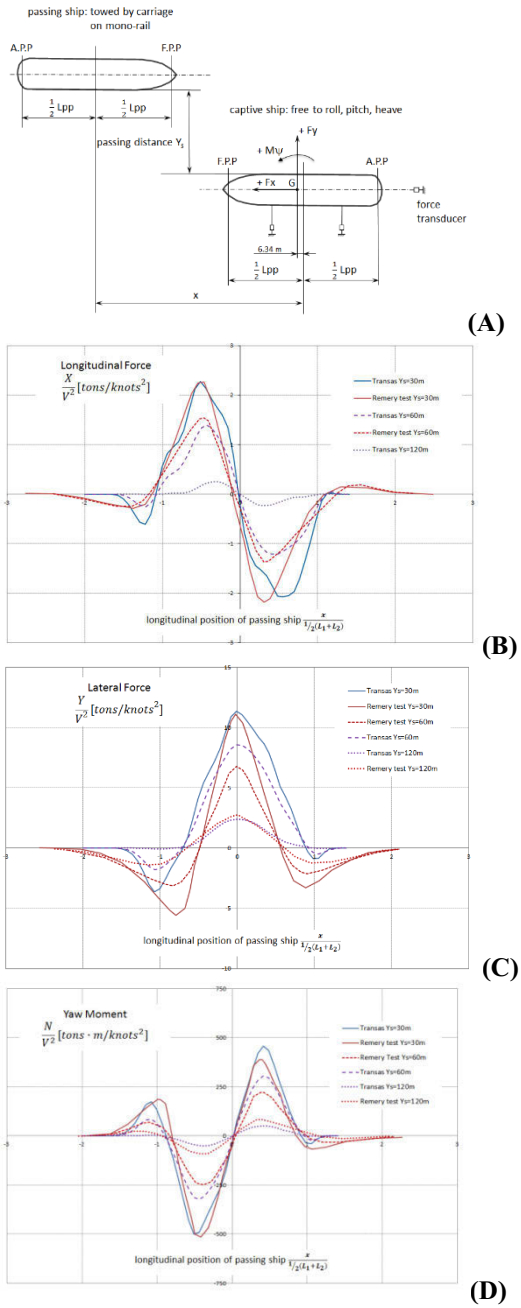


**Figure 11. A – Test set-up for force measurement on captive vessel (according to [16]). B, C, D – Forces induced by passing ship.**

## 5 REPRESENTATION OF THE PREDICTED TRAJECTORY

The predicted trajectory data contains the following information, which can be important for an operator:

- predicted ship positions over pre-set period of time
- possibility of grounding or mechanical interaction along the trajectory
- UKC along the trajectory
- magnitude of interaction forces along the trajectory.

This information can be important for proper ship handling if some of these parameters are close to critical. Also, a set of trajectories can be generated depending on the following expectations:

- all controls will be left as they are now
- rudder will ordered hard to port (starboard)
- rudder will ordered hard to port (starboard) and full speed ahead will be ordered
- full thruster power will be applied to port (starboard)
- full speed astern will be ordered with or without additional steering.

All these options form a space of potential manoeuvres available to the operator, and it could be useful to display some or all of them to make decision making more reliable. However, if all these options will be used simultaneously the user will be overloaded with information and that will prevent decision-making.
Trajectories of other vessels can also be represented in different ways:

- keeping existing course and speed
- keeping existing rate of turn and speed
- use trajectory received from external sources (e.g. e-Navigation).

In figure 12 the example of predicted trajectory representation is shown. The purple dashed line represents ship position at which UKC is below the given limit or hydrodynamic interaction forces will be higher than the available rudder capabilities. The three trajectories shown in the figure 12 represent the full range of ship manoeuvring capabilities. The default assumption that rudder order will remain the same for next few minutes is represented as central black trajectory, while red and green trajectories represent assumptions that hard to port or starboard order will be executed.

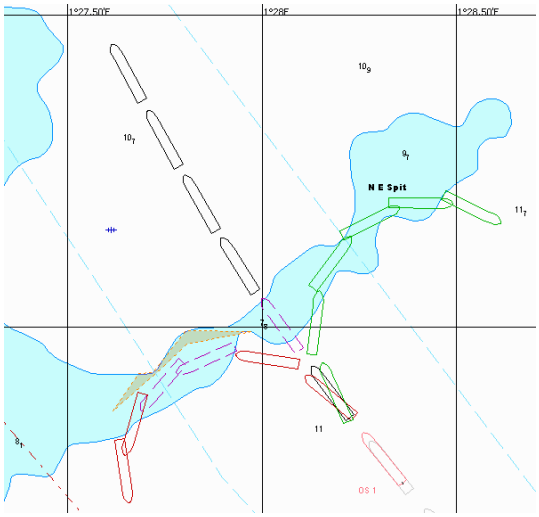


**Figure 12. Representation of predicted trajectory.**

## 6 SIMULATION EXPERIMENT

An experiment was conducted in a simulated Transas NTPro environment to analyse the efficiency of the motion prediction system's support for emergency navigational situation analysis and on-board decision making.
The simulated situation is shown in figure 13. The simulated ship is about to enter the narrow part of the channel after the turn, but the ship moving in the same direction experiences a rudder jam and becomes grounded at the northern entrance to the channel

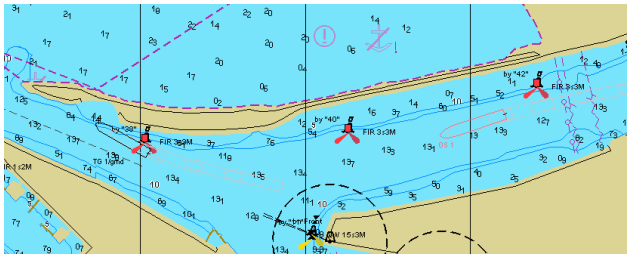

**Figure 13. Simulated manoeuvre: ship TG1 (left, black) is grounded during turn, ship OS1 (right, red) is approaching the turn. At 1:10000 scale.**

In every simulation experiment, a participant was operating OS 1 ship while authors controlled all other ships. . Before the simulation participant was instructed to make the safest decision in a potentially dangerous situation that will happen during the training session, as shown in figure 12. Some trainees were professional mariners, while others were naval architects without ship handling experience. All trainees had 20 minutes introductory training to get used to ship manoeuvring characteristics. The result of each simulation session was estimated as one of three possible cases: collision with channel boundary or other vessel, soft grounding or safe manoeuvre.

**Table 4. Results of simulation experiment**

| | Prediction of own ship | |
|---|---|---|
| | Predictor (1st attempt) | None (2nd attempt) |
| Manoeuvring result (group of 3 naval architects) | | |
| Collison with boundary or vessel | 2 | 1 |
| Soft grounding | 1 | 0 |
| Safe passage | 0 | 2 |
| Average time for safe passage case, min | n/a | 9:15 |
| Manoeuvring result (group of 3 mariners) | | |
| Collison with wall or vessel | 0 | 0 |
| Soft grounding | 0 | 1 |
| Safe passage | 3 | 2 |
| Average time for safe passage case, min | 16:55 | 13:36 |

Though the number of participants was relatively small, some preliminary conclusions could be suggested after analysis of trajectories and results of these experiments:

- Use of the advanced predictor for skilled users forced them to decrease speed in advance and proceed in a safer way, thus reducing the possibility of rough errors.
- Unskilled trainees gain more from their previous experience than from the use of advanced navigation tools.

## 7 CONCLUSIONS

- The developed mathematical model allows fast-time simulation of ship motion considering shallow water effects and simplified model of hydrodynamic interaction between ship and its environment.
- Access to high precision and up-to-date navigational charts is essential for prediction considering mechanical and hydrodynamic interaction.
- Different representation forms of predicted trajectory may provide additional information about future manoeuvre.
- Usage of motion prediction tool is useful for skilled mariners to evaluate and control ship behaviour. Such tools may become even more useful if prediction exchange between different ships in the area is available.
- Future research can be focused on precision enhancement of the model and on enhancing prediction representation. Additional simulated experiments will provide more information about the optimal amount of information provided by a prediction tool.

## 8 ACKNOWLEDGEMENTS

The authors would like to thank the engineers and mariners who helped and participated in simulation experiments: Alexander Sosonkin, Mikhail Andrianov, Andrey Vasiliev, Alexey Antonov, Petr Sobolev, Dmitry Shilkin, Ivan Cheryrbok, Alexey Vasiliev.

## 9 REFERENCES

1. Nakano, T.; Hasegawa, K. (2013). An Attempt to Predict Manoeuvring Indices Using AIS Data for Automatic OD Data Acquisition. *International Workshop of Next Generation Nautical Traffic Models*, Delft, The Netherlands.

2. Baldauf, M.; Mehdi, R.; Deeb, H.; Schröder-Hinrichs, J. U.; Benedict, K.; Krüger, C.; Fischer, S.; Gluch, M. (2015). Manoeuvring areas to adapt ACAS for the maritime domain. *Scientific Journals of the Maritime University of Szczecin* No.43 (115): pp. 39–47.

3. Benedict, K.; Gluch, M.; Kirchhoff, M.; Schaub, M.; Fischer, S.; Baldauf, M. (2015). Innovative simulation

tools for learning & teaching ships dynamic and investigation of manoeuvring capabilities. *MARSIM2015*, Newcastle, UK.

4. Son, N. S.; Furukawa, Y. (2009). Study on the algorithm of collision avoidance for large container in shallow confined waterway. *International Conference on Ship Manoeuvring in Shallow and Confined Water: Bank Effects*, Ghent, Belgium, R.I.N.A.: pp. 113-120.

5. Wijhe van, H. J.; Janssen, W. D.; Blocken, B. (2015). Wind loads on ships in a complex environment. *MARSIM2015,* Newcastle, UK.

6. Fossen, T. I. (2011). *Handbook of Marine Craft Hydrodynamics and Motion Control*. John Wiley & Sons Ltd.: p. 575.

7. Lerner, D. M.; Lukomskiy, Y. A.; Mikhaylov, V. A.; Nornevskiy, B. I.; Petrov, Y. P.; Popov, O. S.; Shleyer, G. E. (1979). *Control of marine moving objects [Upravlenie morskimi podvizhnyimi ob'ektami]*, Shipbuilding [Sudostroenie], Leningrad: p. 271.

8. Voytkunskiy, Y. I., Ed. (1985). *Handbook on ship theory [Spravochnik po teorii korablya] Vol. III*, Shipbuilding [Sudostroenie], Leningrad: p. 544.

9. Vantorre, M. (2001). Manoeuvring coefficients for a container carrier in shallow water: an evaluation of semi-empirical formulae. *Mini Symposium on Prediction of Ship Manoeuvring Performance*, Tokyo, Japan: pp. 71-81.

10. Yoshimura, Y.; Masumoto, Y. (2012). Hydrodynamic database and manoeuvring prediction method with medium high-speed merchant ships and fishing vessels. *MARSIM2012*, Singapore.

11. Brix, J., Ed. (1993). *Manoeuvring technical manual*, Seehafen-Verlag, Hamburg: p. 266.

12. Ankudinov, V. K.; Filippov, I. I.; Sobolev, P. K. (2006). Modeling Of Ship Motions In Restricted Channels On Marine Simulators. *MARSIM2006*, Terschelling, The Netherlands.

13. Sobolev, P. K. (2015). *Basin modeling of ships motion [Basseynovoe modelirovanie dvizheniya sudov]*, Elmore, Saint-Petersburg, Russia: p. 304.

14. Briggs, M. ; Uliczka, K.; Vantorre, M.; Debaillon, P. (2010) Prediction of Squat for Underkeel Clearance. In: *Handbook of Coastal and Ocean Engineering*, Kim, Y. C., Ed., World Scientific, New Jersey: Chapter 26, pp. 723-774.

15. Daggett, L.; Hewlett, C.; Ankudinov , V.; Filippov, I.; Ponomarev, V.; Rogozhina, E.; Shilkin, D. (2009). Application of latest ship maneuvering technology and ship hydrodynamics modeling to the expansion of the panama canal – working out operation procedures and techniques. *MARSIM2009*, Panama City, Panama.

16. Remery, G. F. (1974). Mooring Forces Induced by Passing Ships. *Offshore Technology Conference*, Dallas, Texas: pp. 349-363.

## 10 AUTHORS' BIOGRAPHIES

**Ekaterina Rogozhina** holds the current position of senior expert at Transas Technologies. She is responsible for research in the area of hydrodynamic modelling.

**Alexander Ozersky** holds the current position of section manager at Transas Technologies. He is responsible for algorithm development in the area of hydrodynamic modelling.